Chinese Chemical Letters 37 (2026) 111413

Contents lists available at ScienceDirect

Chinese Chemical Letters

journal homepage: www.elsevier.com/locate/cclet

Controlled assembly of phosphonic acid ligand covalently modified $[TeMo_6O_{21}]^{2-}$ polyanions for proton conduction

Qianqian Liu[a,1], Jianxin Ma[b,1], Lian Xiao[a,1], Shilei Liu[a], Yongzhen Chen[c], Liying Wang[a], Yunzuo Cui[a], Song Liang[c,*], Hong-Ying Zang[a,*]

[a] Key Laboratory of Polyoxometalate and Reticular Chemistry of Ministry of Education Faculty of Chemistry, Northeast Normal University, Changchun 130024, China
[b] School of Chemistry and Environmental Engineering, Changchun University of Science and Technology, Changchun 130022, China
[c] Key Laboratory of Bionic Engineering of the Ministry of Education, College of Biological and Agricultural Engineering, Jilin University, Changchun 130022, China

ARTICLE INFO

Article history:
Received 15 April 2025
Revised 27 May 2025
Accepted 6 June 2025
Available online 6 June 2025

Keywords:
Polyoxometalates
Clusters
In-situ synthesis
Covalent modification
Proton conduction

ABSTRACT

Achieving higher proton conductivity of proton-conducting materials in solid-state is one of the utmost challenges in materials science. Due to their oxygen-rich structure and negative surface charge, polyoxometalates (POMs) anions have high requirements for proton carrier density and proton mobility, and thus have great potential as proton conducting materials. Furthermore, the versatility in modifying the ligand environment or incorporating acidic functional groups in POMs allows for precise tuning of their proton conductivity and stability under operational conditions. Therefore, it is an effective strategy to select a suitable organic ligand to stabilize the $[TeMo_6O_{21}]^{2-}$ anion assembled *in-situ* by covalent modification. In this paper, three $[TeMo_6O_{21}]^{2-}$ anionic clusters have been designed and synthesized by using polydentate phosphonate ligands and guided by transition metals, $H_{26}[Co_6\{N(CH_2PO_3)_2(CH_2COO)\}_6(TeMo_6O_{21})_4(H_2O)_8]\cdot 64H_2O$ (complex **1**), $H_{26}[Cu_6\{N(CH_2PO_3)_2(CH_2COO)\}_6(TeMo_6O_{21})_4(H_2O)_6]\cdot 78H_2O$ (complex **2**) and $H_{34}Na_2[Co_8\{N_2(CH_2)_2(CH_2PO_3)_3(CH_2PO_3H_2)\}_4(TeMo_6O_{21})_6(PO_3)_4(H_2O)_{16}]\cdot 84H_2O$ (complex **3**). Among them, complexes **1** and **2** are isomorphic, and complexes **1–3** have good proton conduction properties, resulting in values of 1.3×10^{-2}, 1.22×10^{-2}, and 1.11×10^{-2} S/cm, respectively (75 % relative humidity, 80 °C). This work offers a promising strategy for the development and design of novel telluromolybdate clusters suitable for proton conductive materials.

© 2026 Published by Elsevier B.V. on behalf of Chinese Chemical Society and Institute of Materia Medica, Chinese Academy of Medical Sciences.

As the core components of clean and green energy technologies such as fuel cells, proton conductor materials have a direct impact on energy transfer efficiency and device stability [1–6]. While traditional perfluorosulfonate polymers (*e.g.*, Nafion) exhibit outstanding proton conductivity, they face the bottleneck problems of high synthesis cost and poor environmental compatibility [7–9]. Therefore, the design and development of new solid materials with high proton conductivity and excellent stability is currently a cutting-edge and hot topic [10–12].

In recent years, metal-organic frameworks (MOFs) [13–15], covalent-organic frameworks (COFs) [16–18], and polyoxometalates (POMs) [19–21] as crystalline porous materials have provided new insights into the design of efficient proton conductors due to their abundant functionalization sites. POMs, a class of multinuclear clusters composed of high-valence transition metals (*e.g.*, Mo, W, V) bridged by shared oxygen atoms [22–27]. Using POMs as proton conductor materials is highly desirable, because (1) the densely distributed oxygen atoms in the POMs skeleton act as hydrogen bond acceptors, which can provide a continuous proton transport channel by forming a dynamic hydrogen bonding network with water molecules or proton carriers [28]; (2) strong Brønsted acidic sites can release H^+ *via* dissociation of -OH groups or H_2O adsorption, which significantly reduces the activation energy of proton conduction and promotes rapid proton transport [29]; (3) POMs can be surface functionalized (*e.g.*, by joining carboxylic acid, phosphonic acid, sulfonic acid groups) or compounded with other materials [30]. The –OH groups in organic ligands serve as both proton sources and proton-hopping sites, providing an effective strategy for constructing high proton conductivity.

* Corresponding authors.
E-mail addresses: songliang@jlu.edu.cn (S. Liang), zanghy100@nenu.edu.cn (H.-Y. Zang).
[1] These authors contributed equally to this work.

https://doi.org/10.1016/j.cclet.2025.111413
1001-8417/© 2026 Published by Elsevier B.V. on behalf of Chinese Chemical Society and Institute of Materia Medica, Chinese Academy of Medical Sciences.

Telluromolybdates as a member of POMs, Anderson-type derivatives of $[Te^{VI}Mo_6O_{24}]^{6-}$ have been extensively researched in recent years. In contrast, the $[TeMo_6O_{21}]^{2-}$ anion sandwiched by Te^{IV} is relatively rare [31,32]. From a structural point of view, Te^{IV} is more interesting due to its richer coordination pattern, such as $\{TeO_3\}$ triangular pyramids, $\{TeO_4\}$ and $\{TeO_5\}$ square pyramids. In recent years, it has been found that the inherent strong coordination ability and multiproton dissociation properties of the phosphonate moiety enable it to form highly nucleated molybdenum-based clusters by precisely anchoring the *in-situ* synthesized $[TeMo_6O_{21}]^{2-}$ polyanions *via* covalent bonds [33–35].

In response to the above challenges, the covalent integration strategy of phosphonic acid ligands with POMs shows unique advantages. Fortunately, we have successfully synthesized three telluromolybdates derivatives covalently modified by phosphonic acid groups through using polydentate phosphonic acid ligands, $H_{26}[Co_6\{N(CH_2PO_3)_2(CH_2COO)\}_6(TeMo_6O_{21})_4(H_2O)_8]\cdot 64H_2O$ (complex **1**), $H_{26}[Cu_6\{N(CH_2PO_3)_2(CH_2COO)\}_6(TeMo_6O_{21})_4(H_2O)_6]\cdot 78H_2O$ (complex **2**) and $H_{34}Na_2[Co_8\{N_2(CH_2)_2(CH_2PO_3)_3(CH_2PO_3H_2)\}_4(TeMo_6O_{21})_6(PO_3)_4(H_2O)_{16}]\cdot 84H_2O$ (complex **3**). The synergistic action of rich oxygen atoms in POMs and phosphonic acid groups creates a continuous hydrogen bond network in complexes **1**–**3**, which realizes directional and rapid proton migration and promotes proton conduction. This work undoubtedly provides a new idea for designing and synthesizing new telluromolybdates. It provides a theoretical basis and material platform for the development of a new generation of high-stability solid-state proton conductors.

Telluromolybdates were synthesized *in-situ* at room temperature by heating NaAc-HAc buffer solution containing organophosphonate ligands, molybdenum source, Na_2TeO_3 and transition metal linking agent, according to the procedure in Supporting information.

An interesting finding is that the formation of $\{TeO_3\}$ trigonal pyramids when introducing the Te^{IV} anion further triggers the formation of the $[TeMo_6O_{21}]^{2-}$ anion from the $\{Mo_2\}$ unit by means of a co-angle linkage. This is distinct from the incorporation of the Te^{VI} anion, which leads to the formation of the Anderson-type $[TeMo_6O_{24}]^{6-}$ anion by linking the $\{Mo_2\}$ units by way of a co-edge connection (Fig. 1). $[TeMo_6O_{21}]^{2-}$ is a rational inorganic scaffold that enables the construction of organophosphonate-functionalized POMs by covalent linkage of phosphonic/carboxylic acid groups.

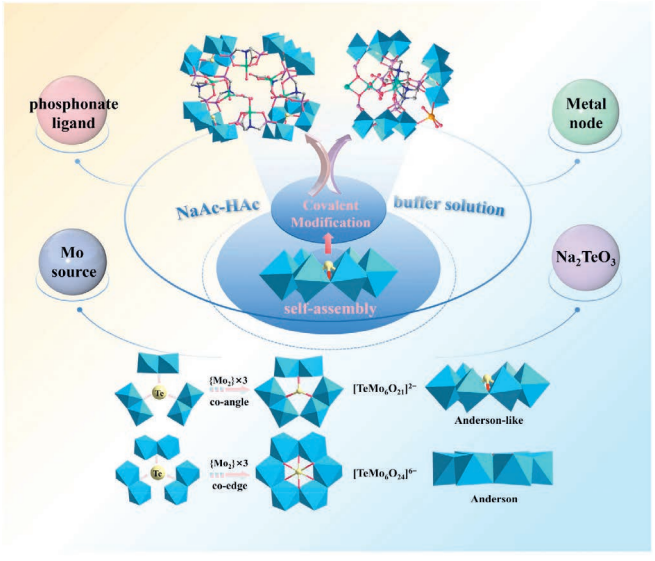


Fig. 1. Self-assembly of $[TeMo_6O_{21}]^{2-}$ and synthesis diagram of complexes **1**–**3**.

To achieve this, we have designed and synthesized complexes **1**–**3** based on Anderson-like-type polymolybdenum clusters using an *in-situ* synthesis method by introducing Te^{IV} anion into the ammonium molybdate system. In addition, the design and selection of organophosphonic acid ligands is also an effective strategy. The phosphonic acid and carboxylic acid groups not only have strong coordination ability, which helps to coordinate with Mo atoms in $[TeMo_6O_{21}]^{2-}$ anions through their oxygen atoms *via* covalent bonds but also can expose more acidic functional groups, which can be used as proton sources and proton hopping sites for the construction of proton-conducting substances with high proton conductivity. The crystal structures of molybdenum-based clusters **1**–**3** were clearly elucidated by single-crystal X-ray crystallography (Table S1 in Supporting information). Isomeric **1** and **2** differ except for the transition metals and the amount of water, therefore the structures of complex **2** are described only by complex **1**.

Complex **1** crystallizes in the *C*2/*c* space group and consists of the tetrameric anion $[Co_6\{N(CH_2PO_3)_2(CH_2COO)\}_6(TeMo_6O_{21})_4(H_2O)_6]^{26-}$ (**1a**), 62 crystallization water molecules, and 26 protons. XPS analysis indicates that all Mo atoms are in the 6+ oxidation state (Fig. S1 in Supporting information).

In complex **1**, Te^{VI} serves as an anionic template located slightly above the $\{MoO_6\}$ unit to form the trigonal pyramids geometry $\{TeO_3\}$, which serves as a template unit to facilitate the *in-situ* synthesis of the $[TeMo_6O_{21}]^{2-}$ anion. The Mo–O distances range from 1.698(6) Å to 2.290(5) Å, the Te–O bond lengths range from 1.873(4) Å to 1.866(4) Å (Fig. 2a). Three crystallographically independent Co atoms (Co1, Co2, and Co3) are present within **1** and adopt the same five-coordination pattern. The Co atoms chelate two phosphonate groups, a carboxyl group, an N atom, and a water molecule of the glyphosine ligand to constitute the $\{Co(N(CH_2PO_3)_2(CH_2COO)(H_2O)\}$ unit (Fig. 2b), which is formed by its two phosphonate groups of the oxygen atoms covalently linked to the Mo1, Mo2 atoms on the $[TeMo_6O_{21}]^{2-}$ anion to form the dimerized $[Co\{N(CH_2PO_3)_2(CH_2COO)\}(TeMo_6O_{21})_2(H_2O)]$ unit (Fig. 2c).

The $[TeMo_6O_{21}]^{2-}$ anion contains three $\{Mo_2\}$ building blocks for covalent attachment of the three phosphonate groups (Fig. 2d). In this way, all P atoms are connected to Mo atoms *via* the

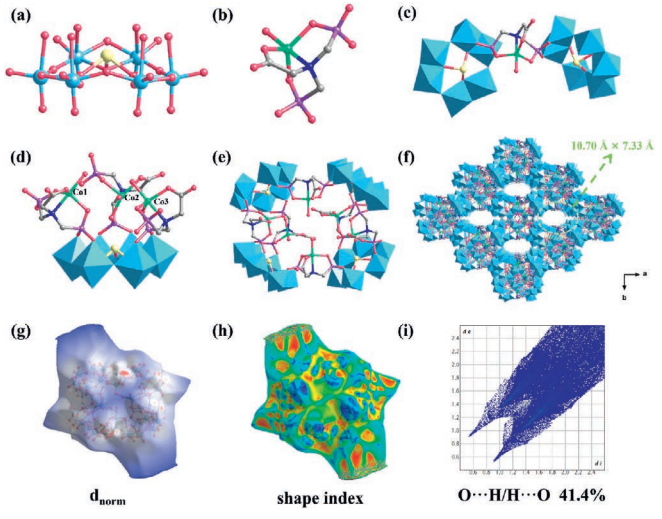


Fig. 2. (a) Ball-and-stick representation of $[TeMo_6O_{21}]^{2-}$. (b) Coordination environment diagram of Co atom. (c) Structure diagram of the dimer $[Co\{N(CH_2PO_3)_2(CH_2COO)\}_6(TeMo_6O_{21})_2(H_2O)]$ unit. (d) Coordination patterns of the $[TeMo_6O_{21}]^{2-}$. (e) The polyanionic skeleton of **1a**. (f) Three-dimensional (3D) stacking diagram of **1** along the *c*-axis. Color code: Mo, light blue; Te, yellow; Co, green; P, purple; O, rose red; C, gray; N, blue. Hirshfeld surface of **1a**: (g) Dnorm map, (h) shape index map. (i) The 2D fingerprint plots of **1a**.

bridge μ_2-oxo ligands of $\{PO_3\}$ groups. The P–O lengths of the $\{PO_3\}$ groups are in the ranges of 1.522(5)–1.541(5) Å (Table S2 in Supporting information). Furthermore, the glyphosine ligand serves as the backbone of the tetramer, with four $\{Co(N(CH_2PO_3)_2(CH_2COO)(H_2O)\}$ units connecting two adjacent dimeric units to form the tetramerized complex **1** (Fig. 2e).

The packing diagram of complex **1** of the tetramer along the *c*-axis (Fig. 2f), exhibits an ordered arrangement of pore structures. The Hirschfeld surface analysis of **1a** is shown in Figs. 2g–i, where different colors in the dnorm and shape index plots reveal different intermolecular interactions. The 2D fingerprint plots of **1a** have an O···H/H···O ratio of 41.4%, suggesting that there is an abundance of hydrogen bonding interactions between the **1a** molecules [36,37]. The contributions of other elements are shown in Fig. S2 (Supporting information).

When EDTMPA ligand was utilized as the organic components, complex **3** was isolated, which crystallized in the *P*-1 space group. The reason for replacing the ligand is that the EDTMPA ligand not only still has the ability to chelate transition metals, but also has more $\{PO_3\}$ groups in its structure available for covalent attachment to the Mo atom in the $[TeMo_6O_{21}]^{2-}$ anion. Complex **3** includes $Na_2[Co_8\{N_2(CH_2)_2(CH_2PO_3)_3(CH_2PO_3H_2)\}_4(TeMo_6O_{21})_6(PO_3)_4(H_2O)_{16}]^{34-}$ (**3a**), 84 crystallization water molecules, 2 Na^+ cations, and 34 protons.

In complex **3**, The "template" $\{TeO_3\}$ connects $\{MoO_6\}$ units to comprise $[TeMo_6O_{21}]^{2-}$ anion. The Te-O bond lengths vary from 1.826(8) Å to 1.892(8) Å, while the Mo-O spacings range from 1.669(10) Å to 2.354(9) Å. Four crystallographically independent Co atoms (Co1, Co2, Co3, and Co4) form complex **3**. Co1 and Co2 each chelate an EDTMPA using the same six-coordination pattern. In detail, the Co1 and Co2 atoms are each coordinated to two nitrogen atoms and four phosphonate oxygens in an EDTMPA to form the {Co(EDTMPA)} unit (Fig. 3a). The {Co1(EDTMPA)} unit and {Co2(EDTMPA)} are covalently linked to the Mo atom in the $[TeMo_6O_{21}]^{2-}$ anion through the uncoordinated oxygen atom in their $\{PO_3\}$ groups to form the trimerized $[Co_2\{N_2(CH_2)_2(CH_2PO_3)_3(CH_2PO_3H_2)\}_2(TeMo_6O_{21})_3(H_2O)_2]^{22-}$ anion cluster (Fig. 3b). The oral trimeric anion cluster is further covalently attached to two opposing $[TeMo_6O_{21}]^{2-}$ anion *via* $\{Co_2(PO_3)_2(H_2O)_4\}$ units to form the $Na[Co_4\{N_2(CH_2)_2(CH_2PO_3)_3(CH_2PO_3H_2)\}_2(TeMo_6O_{21})_3(PO_3)_2(H_2O)_8]^{17-}$ anion (**3b**) (Fig. 3c). Interestingly, two **3b** units can be joined by Na atoms to form **3a** anion clusters (Fig. 3d). Fig. 3e presents the stacking diagram of 3a along the *a*-axis. The Hirschfeld surface analysis of **3a** is shown in Figs. 3f–h and the 2D fingerprint plots of **3a** have an O···H/H···O ratio of 44.8%, suggesting that there is an abundance of hydrogen bonding interactions between the **3a** molecules.

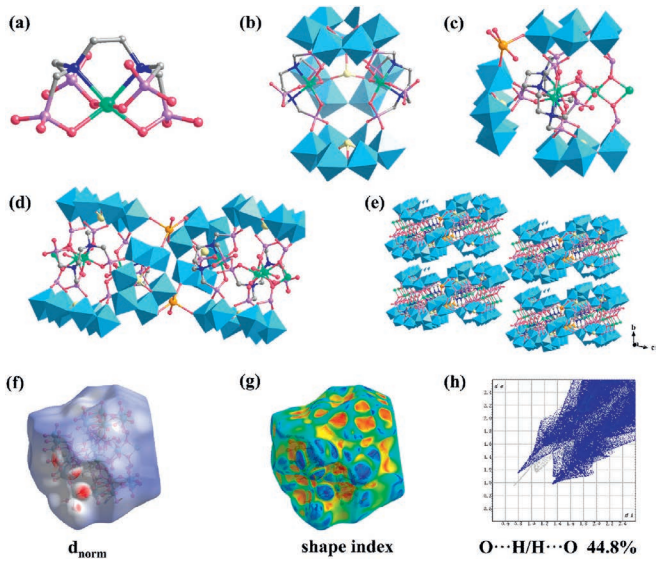


Fig. 3. (a) Ball-and-stick diagrams for {Co(EDTMPA)} unit. (b) $[Co_2\{N_2(CH_2)_2(CH_2PO_3)_3(CH_2PO_3H_2)\}_2(TeMo_6O_{21})_3(H_2O)_2]^{22-}$ anion. (c) **3b** anion structure diagrams. Color code: Mo, light blue; Te, yellow; Co, green; P, purple; O, rose red; C, gray; N, blue; Na, orange. (d) The polyanionic skeleton of **3a**. (e) 3D stacking diagram of **3** along the a-axis. Hirshfeld surface of **3b**: (f) Dnorm map, (g) shape index map. (h) The 2D fingerprint plots of **3b**.

The presence of a large number of disordered crystalline water molecules in complexes **1**–**3**. The SQUEEZE program was used to further approximate the number of crystalline water molecules present in the structure was determined and added to the molecular formula in a theoretical manner. Understanding and predicting the assembly process of novel complexes is not an easy task, and the use of ligands of different configurations to influence the structure of complexes provides a new perspective on the self-assembly process. As expected, the $[TeMo_6O_{21}]^{2-}$ anion formed based on the template "trapping" can be further supported by the backbone of polydentate phosphonate/carboxylic acid ligands to form tetrameric complexes **1**, **2** and hexameric **3**. This provides a rational basis as well as an approach to enrich the diversity of the family of novel Telluromolybdates. We performed extensive powder X-ray diffraction (PXRD), FT-IR, thermogravimetric analysis, and scanning electron microscopy (Figs. S3-S8 in Supporting information) to demonstrate the phase purity, chemical structure, and stability of complexes **1**–**3**. The PXRD of simulated **1**–**3** corroborates the measured data indicating the good phase purities of **1**–**3**.

POM clusters with a high density of oxygen sites can form an effective hydrogen bonding network with guest molecules and water molecules. Their well-ordered crystallinity and Brønsted acidity can provide abundant proton hopping sites and binding sites for proton transfer [38]. It is recognized that water adsorption is a useful method to study the affinity of materials for water and that the water adsorption capacity is closely related to proton conduction studies [39]. Complexes **1**–**3** exhibited a stepwise increase in water adsorption with increasing relative humidity at 25 °C (Fig. S9 in Supporting information). The maximum adsorption capacities of **1**–**3** were 215.8, 225.1, and 249.1 mg/g, respectively, which further verified that **1**–**3** possessed desirable storage capacity for water molecules.

In order to evaluate the worth of complexes **1**–**3** as a solid electrolyte, the proton conductivity (σ) properties of **1**–**3** were measured at different relative humidity (RH) and temperatures using the AC impedance technique. Firstly, the σ variations of **1**–**3** at different RH were investigated at 303 K (Fig. S10 in Supporting information). The experimental results revealed that the σ of **1**–**3** aggrandized from 2.68×10^{-5}, 7.69×10^{-5}, and 5.48×10^{-5} S/cm to 5.71×10^{-4}, 9.38×10^{-4}, and 1.02×10^{-3} S/cm, respectively (Table S4 in Supporting information), when the RH was increased from 55% to 75% (Fig. 4a). It can be attributed to the high content of oxygen atoms on/in the surface of the POMs, and the phosphonic acid/carboxylic group on the ligand establishes an extensive hydrogen bonding network with the adsorbed water molecules, accelerating the proton transfer and thus significantly enhancing the σ.

It is well-recognized that temperature can affect the migration rate of proton carriers and is critical for the enhancement of σ. We investigated the changes in σ of **1**–**3** in the temperature range of 30–80 °C at 75% RH. The Nyquist plots of the tests (Fig. S11 in Supporting information) demonstrated that the measured resistance gradually decreased with the increase in temperature. Meanwhile, the σ tends to increase with increasing temperature (Fig. 4b). At 80 °C, the σ values of **1**–**3** reached 1.3×10^{-2}, 1.22×10^{-2}, and 1.11×10^{-2} S/cm (Table S5 in Supporting information), which is attributed to the forming of H_3O^+ by H_2O and H^+ at higher temperatures, thus improves the proton conduction.

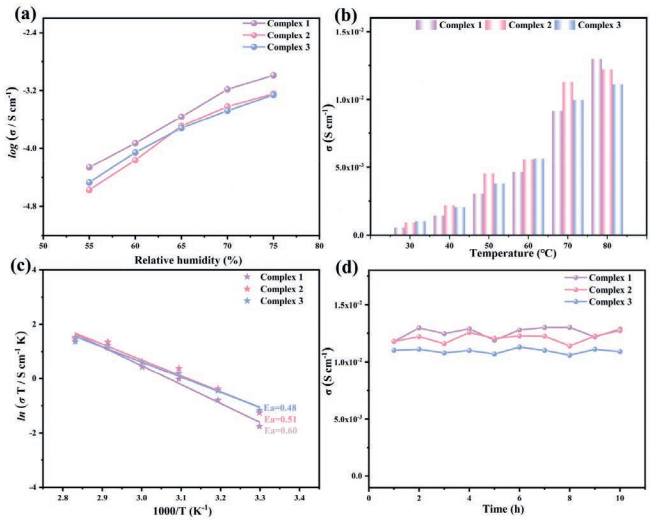


Fig. 4. (a) Humidity-dependent σ at 30 °C (55 %–75 % RH). (b) Temperature-dependent σ at 75 % RH (30–80 °C). (c) Arrhenius plots of the proton conductivity of **1**–**3** clusters. (d) Time-dependent σ at 75 % RH and 80 °C.

The proton conductivity (σ) is primarily influenced by three key factors: (1) The concentration of protons; (2) the count; and (3) the mobility of carriers or sites. POMs are rich in proton hopping sites and contain a multitude of removable protons and carriers for fast charge transfer [28,40,41]. When coupled with tight and widespread hydrogen bonding, POMs have been discovered to be very efficient at facilitating proton transfer. To date, the Grotthuss and vehicular mechanisms are the two widely accepted mechanisms in solid-state electrolytes. In particular, E_a values below 0.4 eV are generally assigned to the Grotthuss mechanism, in which potons follow an ordered path through a network of water molecules or hydrogen bonds. For vehicular mechanism, the E_a values are typically greater than 0.4 eV, as it involves hydrogen proton transfer occurring in the form of large vehicles, which require larger energy [42,43]. To discover the proton conduction mechanism of **1**–**3**, we fitted σ at different temperatures to the Arrhenius equation. The activation energies (E_a) of **1**–**3** were calculated to be 0.60, 0.51, and 0.48 eV, respectively, indicating that **1**–**3** follow the vehicular mechanism (Fig. 4c).

Due to the fact that **1**–**3** are molybdenum-based clusters constructed on the basis of $[TeMo_6O_{21}]^{2-}$ anions, metal-centered, and phosphonic acid ligands. Complexes **1**–**3** all contain a large number of crystalline water molecules as well as hydrogen protons, which endow them with high proton conductivity. The favorable proton conductivity properties of **1**–**3** can be accounted for by the rapid transport of protons carried by water molecules as carriers. Compared to **1** and **2**, **3** has more Mo nuclei, unsaturated coordinated $\{PO_3\}$ groups, and better water adsorption ability, a fusion that casts **3** with excellent conductivity of protons as well as smaller E_a. The schematic diagrams of the possible proton conduction mechanisms of complexes **1** and **3** are depicted in Fig. S12 (Supporting information).

In addition, the Hebb-Wagner direct current polarization method [44] was used to investigate time-dependent current profiles of **1**–**3**. At a constant voltage of 0.1 V, the resistances of **1**–**3** were 6.9×10^7, 9.17×10^7, and 9.62×10^7 Ω, respectively (Fig. S13 in Supporting information). The results verify that **1**–**3** mainly contribute to proton conduction rather than electron conduction. Evaluating the stability of proton conductors is an important factor in evaluating practical applications. After 10 h of continuous testing of complexes **1**–**3**, the proton conductivity of **1**–**3** remained relatively stable (Fig. 4d). Subsequently, IR (Fig. S14 in Supporting information) and PXRD (Fig. S3) procedures were used to verify the stability of the materials. The results showed good IR and PXRD agreement before and after the test and also proved that the **1**–**3** have good cyclic stability.

In conclusion, we have explored an *in-situ* synthesis method based on the template "trapping" of $\{TeO_3\}$ triggered $[TeMo_6O_{21}]^{2-}$ anion, which is a self-assembly process of molybdenum clusters guided by polydentate phosphonate ligands and transition metals, and obtained three clusters of Telluromolybdates clusters with the targeted geometries. The structures of complexes **1**–**3** were comprehensively characterized and their proton conductivity was studied in detail. Complexes **1**–**3** exhibit strong water absorption and superprotonic conductivity over 10^{-2} S/cm, providing a feasible approach for designing POMs materials with high proton conductivity. This work opens up new insights into the design and development of novel proton conduction materials.

CRediT authorship contribution statement

Qianqian Liu: Writing – original draft. **Jianxin Ma:** Writing – review & editing. **Lian Xiao:** Data curation. **Shilei Liu:** Validation. **Yongzhen Chen:** Methodology. **Liying Wang:** Software. **Yunzuo Cui:** Formal analysis. **Song Liang:** Writing – review & editing, Funding acquisition. **Hong-Ying Zang:** Writing – review & editing.

Declaration of competing interest

The authors declare that they have no known competing financial interests or personal relationships that could have appeared to influence the work reported in this paper.

Acknowledgments

This work was supported by the National Natural Science Foundation of China (No. 22322102), the Fundamental Research Funds for the Central Universities-Excellent Youth Team Program (No. 2412023YQ001), the Natural Science Foundation of Jilin Province (No. 20200201083JC), the Natural Science Foundation of the Department of Education of Jilin Province (No. JJKH20201169KJ).

Supplementary materials

Supplementary material associated with this article can be found, in the online version, at doi:10.1016/j.cclet.2025.111413.

References

[1] I.E.L. Stephens, J. Rossmeisl, I. Chorkendorff, Science 354 (2016) 1378–1379.
[2] J. Zuo, N.Y. Steiner, Z.L. Li, D. Hissel, Renew. Sustain. Energy Rev. 201 (2024) 114613.
[3] W.X. Zhang, S.Q. Zhao, R. Wang, et al., Adv. Compos. Hybrid Mater. 6 (2023) 60.
[4] S.L. Zheng, C.M. Wu, L.H. Chung, et al., ACS Energy Lett. 8 (2023) 3095–3101.
[5] S.Y. Liu, X.X. Li, W.C. Chen, et al., Sci. China Chem. 67 (2024) 862–868.
[6] S.C. Pal, D. Mukherjee, R. Sahoo, S. Mondal, M.C. Das, ACS Energy Lett. 6 (2021) 4431–4453.
[7] K.A. Mauritz, R.B. Moore, Chem. Rev. 104 (2004) 4535–4586.
[8] S.C. Pal, M.C. Das, Adv. Funct. Mater. 31 (2021) 2101584.
[9] S.J. Wang, M. Wahiduzzaman, L. Davis, et al., Nat. Commun. 9 (2018) 4937.
[10] X.M. Li, J.C. Jia, D.T. Yang, J.L. Jin, J.K. Gao, Chin. Chem. Lett. 35 (2024) 108474.
[11] S.C. Pal, D. Mukherjee, Y. Oruganti, et al., J. Am. Chem. Soc. 146 (2024) 14546–14557.
[12] Z.Y. Yang, N.J. Zhang, L. Lei, et al., JACS Au 2 (2022) 819–826.
[13] G. Wang, J.L. Li, H.B. Li, et al., Chin. Chem. Lett. 34 (2023) 107497.
[14] A.L. Li, Q. Gao, J. Xu, X.H. Bu, Coord. Chem. Rev. 344 (2017) 54–82.
[15] J.X. Ma, C. Wang, Q.Q. Liu, et al., Adv. Funct. Mater. 35 (2025) 2419752.
[16] L.Q. Hao, E. Lin, J.J. Liu, et al., Small 21 (2025) 2411954.
[17] T.Y. Qiu, T.H. Wang, W.S. Tang, et al., Angew. Chem. Int. Ed. 62 (2023) e202312020.
[18] S.S. Liu, Q.Q. Liu, S.Z. Huang, et al., Coord. Chem. Rev. 451 (2022) 214241.
[19] N. Ogiwara, T. Iwano, T. Ito, S. Uchida, Coord. Chem. Rev. 462 (2022) 214524.

[20] A. Saha, R. Sahoo, S.C. Pal, S. Uchida, M.C. Das, ACS Energy Lett. 10 (2025) 1958–1998.
[21] J. Geng, Y. Lu, J.Q. Yang, et al., Chem. Eng. J. 511 (2025) 161798.
[22] H.Y. Wang, H. Xu, C.L. Chen, et al., Chin. Chem. Lett. 35 (2024) 108486.
[23] L.Z. Qiao, M. Song, A.F. Geng, S. Yao, Chin. Chem. Lett. 30 (2019) 1273–1276.
[24] Y.C. Liu, X.G. Zhou, T.Y. Qiu, et al., Adv. Mater. 36 (2024) 2407705.
[25] J. Li, Y.Q. Feng, F.Y. Fu, et al., Chin. Chem. Lett. 35 (2024) 108736.
[26] Y.Q. Feng, F.Y. Fu, L.L. Zeng, et al., Angew. Chem. Int. Ed. 63 (2024) e202317341.
[27] Q. Li, F.Y. Fu, M.Y. Zhao, et al., Chin. Chem. Lett. 36 (2025) 110090.
[28] T. Iwano, D. Akutsu, H. Ubukata, et al., J. Am. Chem. Soc. 146 (2024) 26113–26120.
[29] R.L. Liu, Y.F. Chen, X. Su, et al., Coord. Chem. Rev. 522 (2025) 216224.
[30] H. Zhang, S.W. Wang, E.M. Lv, et al., Energy Environ. Sci. 18 (2025) 3986–4009.
[31] Y.F. Liang, S.Z. Li, D.H. Yang, et al., J. Mater. Chem. C. 3 (2015) 4632.
[32] B.J. Xu, Z.H. Liu, Q.F. Xu, et al., J. Mater. Sci. 56 (2021) 4654–4665.
[33] H. Kong, S.Y. Liu, Y.Q. Wang, et al., Inorg. Chem. 60 (2021) 15759–15767.
[34] J.W. Purcell, D.L. Long, E.C. Lee, L. Cronin, H.N. Miras, Dalton Trans. 47 (2018) 6283–6287.
[35] B. Li, X.Z. Duan, Y.Z. Cui, et al., Angew. Chem. Int. Ed. 63 (2024) e202408096.
[36] M.A. Spackman, P.G. Byrom, Chem. Phys. Lett. 267 (1997) 215–220.
[37] M.A. Spackman, D. Jayatilaka, CrystEngComm 11 (2009) 19–32.
[38] X.X. Li, C.H. Li, M.J. Hou, et al., Nat. Commun. 14 (2023) 5025.
[39] Z.W. Jiang, Y.Q. Sun, Y. Rao, et al., Nat. Synth. 4 (2025) 622–631.
[40] B.X. Han, Y.F. Jiang, X.R. Sun, Z.F. Li, G. Li, Coord. Chem. Rev. 432 (2021) 213754.
[41] J.W. Zhong, J.P. Ramírez, N. Yan, Green Chem. 23 (2021) 18–36.
[42] S. Pili, S.P. Argent, C.G. Morris, et al., J. Am. Chem. Soc. 138 (2016) 6352–6355.
[43] W.W. Zou, G.X. Jiang, W.F. Zhang, et al., Adv. Funct. Mater. 33 (2023) 2213642.
[44] T. Miruszewski, K. Dzierzgowski, P. Winiarz, et al., J. Mater. Chem. A 10 (2022) 7218–7227.